International Journal of ISSI, Vol. 15(2018), No. 2, pp. 54-61

Grain Size Effect on the Hot Deformation Processing Map of AISI 304 Austenitic Stainless Steel

J. Rasti *[1]

Department of Mechanical Engineering, Qom University of Technology (QUT), Qom, Iran, Zip: 1519-37195

Abstract

In this study, the hot deformation processing map of AISI 304 austenitic stainless steel in two initial grain sizes of 15 and 40 μm was investigated. For this purpose, cylindrical samples were used in the hot compression test at the temperature ranges of 950-1100 °C and the strain rates of 0.005-0.5% s-1. At first, the relationship between the peak stress and Zener-Hollomon parameter was obtained and their microstructures were studied, then the strain rate sensitivity and the processing map were determined at the strains of 0.5 and 0.7. It was found that in the range of temperature and strain rate studied here, the prevailing softening mechanism is the dynamic recrystallization process. Instability regions were observed at lower temperatures and higher strain rates, associated with the occurrence of necklace phenomena in both grain sizes especially the emphasized semi-necklace structure in the coarse-grained steel, and moreover to the formation of geometrically necessary dislocation along the grain boundaries as well as the development of cell structure interior the grains in the fine grain steel. Results also showed that with increasing temperature and decreasing strain rate, the power dissipation efficiency and the strain rate sensitivity are both increased, indicating an increase in the volume of recrystallized material in a constant strain and a decrease in the susceptibility to the localization of the plastic flow.

Keywords: : Austenitic stainless steel; Dynamic recrystallization; Processing map; Grain size effect.

1. Introduction

The importance and widespread use of stainless steels in the oil, gas and petrochemical industries, as well as food, pharmaceutical and medical engineering industries have created a strong competition in the world market for the production of these types of steel. Among these types, AISI 304 austenitic stainless steel is the most widely used stainless steel due to its high corrosion resistance, good workability, and high toughness at low temperatures. The production of these steels requires a high technical knowledge, involving secondary metallurgy methods such as vacuum oxygen degassing (VOD), qualifying techniques, continuous casting, homogenization, and finally controlled rolling (hot, warm, and cold) to make different sections.

In the hot rolling stage, selection of suitable rolling parameters including temperature, strain rate and strain measure of each pass are based on the appropriate hot workability window on surveying processing map. These maps come from various tests such as torsion, tension,

* *Corresponding author*
Tell: +98 025 36641601
Email: Rasti@qut.ac.ir
Address: Department of Mechanical Engineering, Qom University of Technology (QUT), Qom, Iran, Zip: 1519-37195
1. Assistant Professor

pressure, forging, hammer forging, rolling, and extrusion based on the Dynamic Material Model (DMM) [1-5].

At a given temperature in the hot working regime, the rate of dissipation work (power) is directly proportional to the rate of internal entropy production which is always positive since the process is irreversible. The total rate of entropy production consists of two complementary parts. The first part (generally larger) consists of "conduction entropy" which is due to the conduction of heat from where it is generated (due to plastic flow) to the colder parts of the body (G content). The second part is due to a microstructural dissipation (J co-content) which lowers the flow stress for plastic flow (dislocation movement). Ziegler represented these two in terms of dissipative functions in the velocity and force space and showed that the instantaneously dissipated total power is given by [6]:

$$P_{T,\varepsilon} = \bar{\sigma}\dot{\bar{\varepsilon}} = \mathrm{G} + \mathrm{J} = \int_0^{\dot{\bar{\varepsilon}}} \bar{\sigma} d\dot{\bar{\varepsilon}} + \int_0^{\bar{\sigma}} \dot{\bar{\varepsilon}} d\bar{\sigma} \qquad \text{Eq. (1)}$$

, where $\bar{\sigma}$ and $\dot{\bar{\varepsilon}}$ are equivalent stress and strain, respectively. Figure 1 shows the parameters G and J schematically in the $\bar{\sigma} - \dot{\bar{\varepsilon}}$ plot.

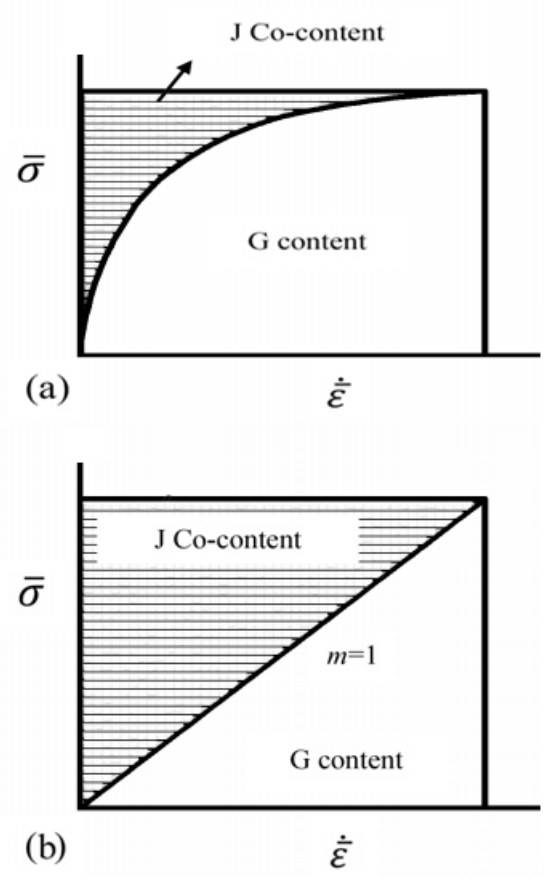

Fig. 1. The parameters G and J in the $\bar{\sigma} - \dot{\bar{\varepsilon}}$ plot in a (a) nonlinear dissipater and (b) ideal linear dissipater (m=1).

In turn, the power dissipation behavior depends on the constitutive equation of the material, which is usually in the form of a power-law relationship as follows:

$$\bar{\sigma} = K\left(T, \bar{\varepsilon}, \dot{\bar{\varepsilon}}\right)\dot{\bar{\varepsilon}}^{\,m\left(T,\bar{\varepsilon},\dot{\bar{\varepsilon}}\right)} \qquad \text{Eq. (2)}$$

, where K is the strength coefficient and m is the strain rate sensitivity exponent. At a given temperature and strain, the parameter J is determined from the following equation:

$$J = \frac{m}{m+1}\bar{\sigma}\dot{\bar{\varepsilon}} \qquad \text{Eq. (3)}$$

This parameter which is belong to the nonlinear material can be normalized by the $J = \frac{1}{2}\bar{\sigma}\dot{\bar{\varepsilon}}$ for the ideal linear material (m=1) to obtain efficiency of power dissipation (η) as follows:

$$\eta = \frac{J}{J_{max}} = \frac{2m}{m+1} \qquad \text{Eq. (4)}$$

The efficiency parameter (η) may be plotted as a function of temperature and strain rate to obtain the power dissipation map. Maps at different strains do not show many differences and the strain components only define the frame of the microsystem [6]. The efficiency parameter describes the relative rate of entropy production occurring during hot deformation due to a microstructural change in the system. Prasad combined the continuity of the metallurgical systems with the DMM and showed the instability in the plastic flow could be observed where the following conditions is satisfied [7]:

$$\xi\left(\dot{\bar{\varepsilon}}\right) = \frac{\partial\left\{\ln\left[m/m+1\right]\right\}}{\partial\left(\ln\dot{\bar{\varepsilon}}\right)} + m < 0 \qquad \text{Eq. (5)}$$

The $\xi\left(\dot{\bar{\varepsilon}}\right)$ parameter may be evaluated as a function of temperature and strain rate to obtain an instability map, where metallurgical instability during plastic flow occurs in regimes where $\xi\left(\dot{\bar{\varepsilon}}\right)$ is negative. The well-known manifestations of flow instabilities are adiabatic shear bands, flow localization, dynamic strain aging (Lüder's bands), kink bands, mechanical twinning and flow rotations. However, the role of these processes in material flow is more important than its nature. For instance, the mechanical twinning, somewhere by the activation of new slip systems, can contribute to plastic flow, which will not cause instability of flow [8, 9]. As a general route, the presence of these instabilities in the microstructure of the component will have

to be avoided by keeping away from the processing conditions of the unstable regimes. It is known that the maximization of η and m in those regions with no instability reduce the tendency for flow localization and material can be deformed to higher extent without risk of abrupt rupture.

The higher hot workability of austenitic stainless steels can be attained in regions that dynamic recrystallization (DRX) is a dominant softening mechanism, i.e. in the range of temperature of 1100-1200 °C [10]. Constitutive equation for the AISI 304 stainless steel has been obtained through torsion test by Ryan and McQueen [11]. The same results have been attained through compression test by Rasti et al. [12]. Venugopal et al. have developed the processing map of this steel to high extent of temperature range of 600-1250 °C and strain rate range of 0.001-100 s^{-1} [13, 14]. They showed that at temperature lower than 1000 °C, flow localization and at temperature higher than 1200 °C, ferrite formation are responsible for flow instability. Furthermore, at temperatures lower than 300 °C the formation of martensite limits the workability of this steel. Although, the results of almost all researches in this context emphasizes that the appropriate range of temperature and strain rate is the region that DRX is dominant softening mechanism, neither the mechanism of development of DRX nor the grain size effect on the processing map of this steel has been studied before. Therefore, the aim of this study is to concern these effects.

Dynamic recrystallization, generally, developes in materials with three mechanisms including discontinuous DRX (d-DRX), continuous DRX (c-DRX), and geometrical DRX (G-DRX) [15-16]. In the discontinuous DRX mode, which is a characteristic of softening mechanism of austenitic stainless steels, the process may be accompanied by necklace structure formation. In this case, newly re-crystallized grains are nucleated and grown along the pre-existence serrated grain boundaries to form a ring (or necklace) of new DRX grains. These grains, which at first have a low density of dislocations, grow rapidly with the deformation of the material, and consequently the dislocation density increases behind the moving boundary, so that finally, the dislocation density difference at two sides of the boundary, as a driving force, becomes so low that the boundary stops and DRX grain size is determined. The formation of the second ring is usually difficult and requires a lot of activation energy because of large curvature of the first ring in DRX grain boundaries. The smaller the initial grain size of the material is, the greater the geometric dislocation density (GNDs) in front of moving DRX boundary through the initial grains is and it causes the DRX grains can grow to some greater size before stopping. Therefore, in materials with a smaller initial grains, due to occurrence of GNDs, usually no necklace structure is involved. With this viewpoint, the initial grain size plays an important role in how DRX extend through the grains and the kinetics of this process.

2. Materials and Method

AISI 304 stainless steel with a chemical composition (wt.%) of Fe-0.033% C-9.07% Ni-18.3% Cr-1.97% Mn-0.342% Si-0.573% Mo-0.075% Ti-0.023% P was used in this study. Cylindrical samples 15 mm in height and 10 mm in diameter were machined from hot rolled bars. The initial grain size of the hot rolled bar was 6 μm, where specimens were annealed at 1100 °C for 5 and 30 min to attain the homogenized microstructure with an average grain size of 15 and 40 μm before deformation. Hot compression tests were then carried out at strain rates of 0.005, 0.05, and 0.5 s^{-1} and temperatures of 950, 1000, 1050, and 1100 °C to the true strain of 1 in order to study the recrystallization behavior during deformation. Mica plates and BN powder were used for lubricating. Samples were quenched immediately (<1 s) after deformation to investigate the DRX microstructures. Samples were then cut along the compression axis and after grinding and polishing etched electrochemically in a 65% nitric acid solution. In order to minimize the effect of friction on the stress – strain curves, the method of Ebrahimi and Najafizadeh was used [17]. To study and plot the processing map, the strains of 0.5 and 0.7 were selected.

3. Results and Discussion

Figure 2 shows the stress-strain curves obtained from the hot compression tests with two initial grain sizes under various deformation conditions. All the samples exhibited typical DRX flow curves with a single peak stress followed by a gradual fall towards a steady state stress. A clear delay for the start of DRX can be observed on the curves corresponding to the large initial grain size (40 μm). In fact, at the highest strain rate tested (0.5 s^{-1}), steady state of the flow stress corresponding to the large grain size was not achieved.

The effect of initial grain size on peak stress is shown in Fig. 3. The activation energy of deformation, Q_{def}, can be estimated by fitting a hyperbolic sine function to the peak stress (σ_p), as first proposed by Sellars and McTegart [18]:

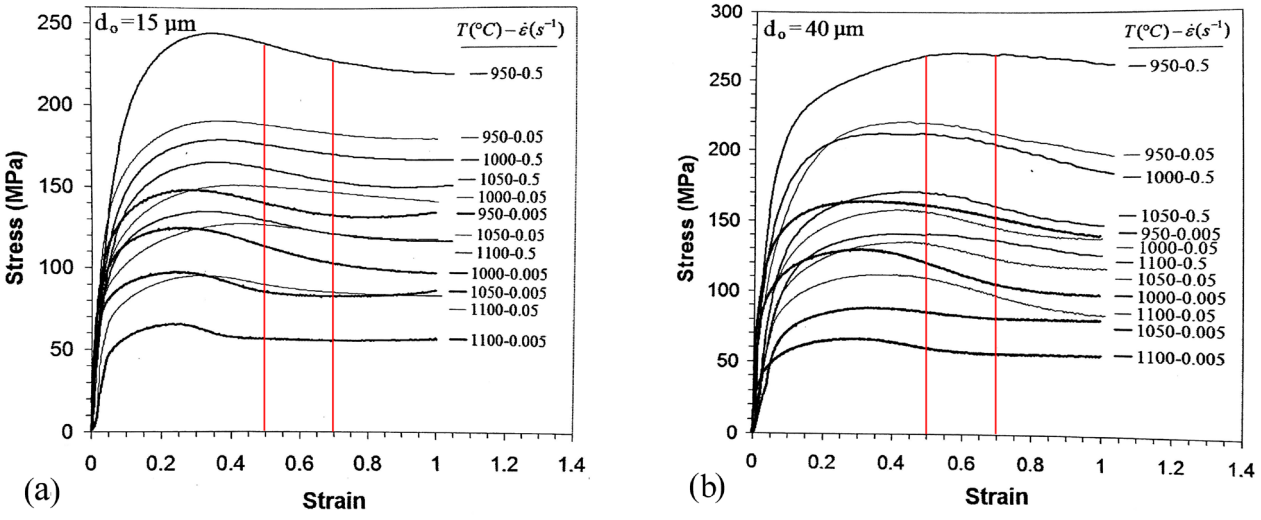

Fig. 2. The stress-strain curves during different conditions of hot deformation in AISI 304 stainless steel at two initial grain sizes of (a) 15 μm, and (b) 40 μm. Vertical lines show the stresses used to delineate processing map.

$$Z = \dot{\varepsilon}\exp(Q_{def}/RT) = A\left(sinh\left(\alpha\sigma_p\right)\right)^n \qquad \text{Eq. (6)}$$

, where Z is the Zener-Hollomon parameter, $\dot{\varepsilon}$ is the strain rate (s^{-1}), A, α, and n are constants independent of temperature, R is the gas constant and T is the absolute temperature (K) of the deformation. Values of 415.7 and 384.1 kJ mol^{-1} were obtained for two initial grain sizes of 40 and 15 μm, respectively, which lie within the range of 370 ~ 470 kJ mol^{-1} reported by others for 304 stainless steel [19].

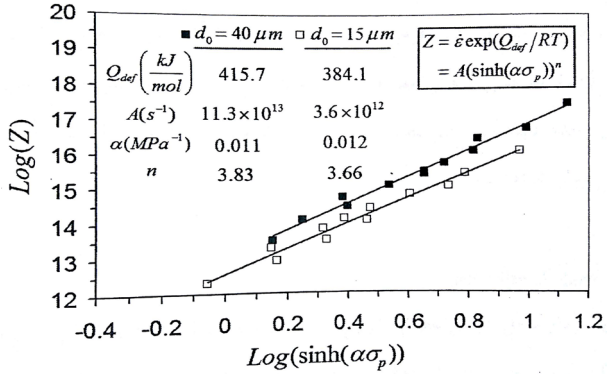

Fig. 3. The peak stress vs. Z parameter in steels with two initial grain sizes.

The less activation energy of deformation in steel with a smaller grain size could be due to the different mechanism of dynamic recrystallization development interior the deformed grains as compared with the larger one. However, in both steels, discontinuous recrystallization occurs but, as it goes on, in coarse-grained steel, a dynamic recrystallization develops further by necklace mechanism. It has also been reported that the nucleation of DRX grains on the serrated boundary is accomplished by two mechanisms including mechanical twinning and subgrain formation, which their dominance could be influenced by the grain size [20].

Fig. 4 shows the development of microstructure in steel with two initial grain sizes of 15 and 40 μm in strain of 1 at different temperatures and strain rates. As can be concluded from the microstructures, DRX developed by necklace mechanism at lower temperatures and higher strain rates (higher Z parameters), especially in steel with a coarser grain size. In finer grain steel, due to the presence of geometrically necessary dislocations (GNDs) and more triple grain boundary junctions, necklace mechanism has less influence on DRX evolution interior initial pancaked grains.

In order to plot the power dissipation efficiency (η) and process map, the strain rate sensitivity (m) was obtained first in terms of strain rate and temperature in a particular strain. Selected strains were 0.5 and 0.7. Stresses were read in these strains and then, using the Table Curve 3D V4.0 software, a 3D curve fitting among the stress logarithm $\ln(\sigma)$, temperature T (°C), and the strain rate logarithm $\ln(\dot{\varepsilon})$ was performed and a mathematical relation obtained. Then, using the relation function of strain rate sensitivity (m) was attained. In the next step, the Surfer 15 software was used to plot the contour curves in power dissipation efficiency charts as well as unstable map plots.

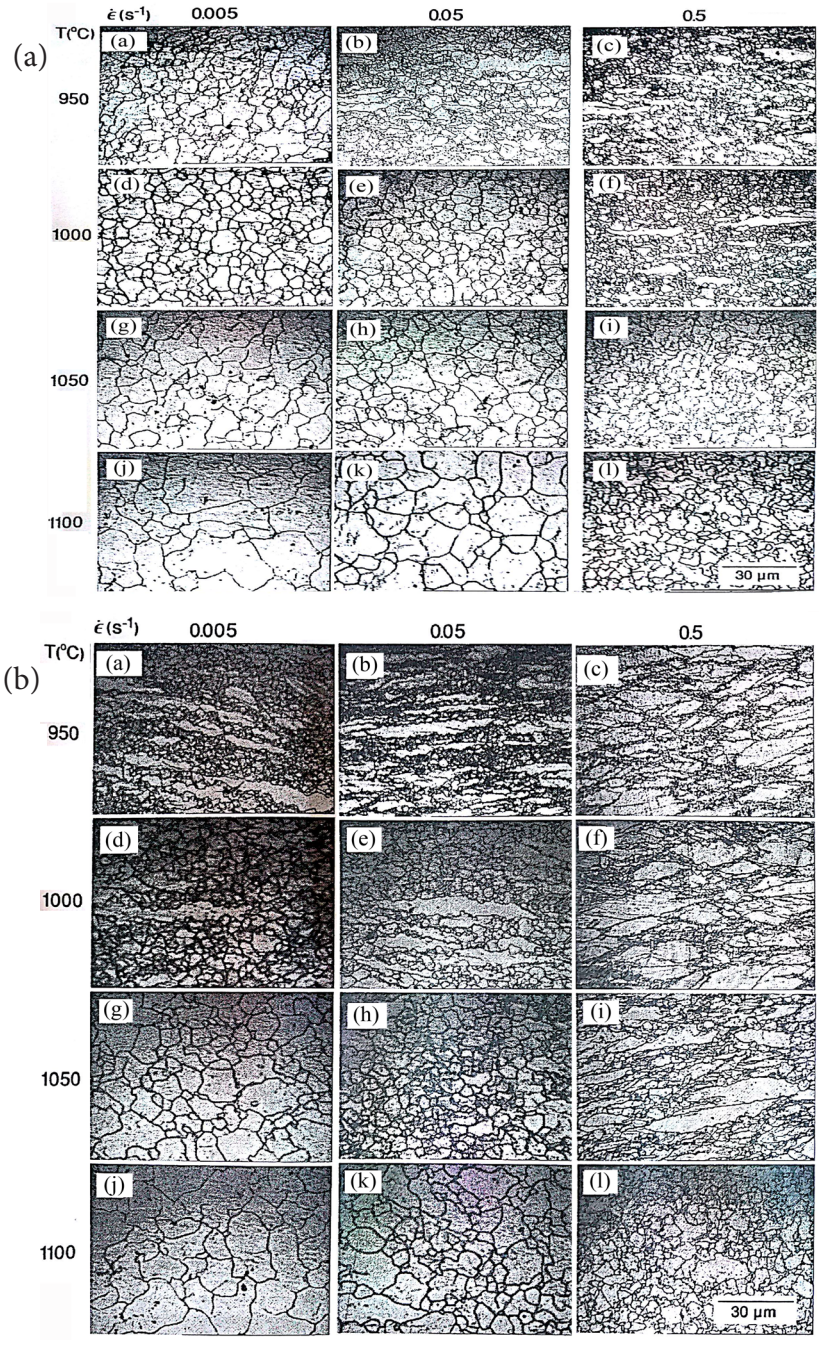

Fig. 4. Microstructural evolution at strain of 1 in steels with two initial grain sizes of (a) 15 μm, and (b) 40 μm at different conditions.

The following relationship among stress, temperature, and strain rate was considered with a goodness-of-fit about R^2= 0.99 in two steel:

Eq. (7)

$$\ln(\sigma) = a + bT + c\ln(\dot{\varepsilon}) + dT^2 + e\left[\ln(\dot{\varepsilon})\right]^2 + fT\ln(\dot{\varepsilon})$$

The parameters a through *f* are constants and obtained by Table Curve 3D V4.0 software. According to the relation $m(T,\dot{\varepsilon}) = \frac{\partial \ln(\sigma)}{\partial \ln(\dot{\varepsilon})}$, the strain rate sensitivity (m) was equal to:

$$m = c + 2e\ln(\dot{\varepsilon}) + fT \qquad \text{Eq. (8)}$$

Fig. 5 (a) – (d) shows the m values obtained in two steels with different grain sizes in strains of 0.5 and 0.7. Due to the positive values of m in all conditions studied here, there should be no instability phenomena such as

shear bands or dynamic strain aging. This issue can be verified by examining the microstructures of Fig. 4. The parameter m, as expected, must also not be meaningful in two different strains [13]. The values of m in two steels with different grain sizes show a general trend. This parameter increases with increasing temperature and decreasing the strain rate (Z decreasing), so that at 950 °C and the strain rate is about 0.05- 0.09 and at temperature of 1100 °C and strain rate of 0.005 s^{-1} reaches about 0.2. Indeed, in term of Z relevance, the following relationships could be obtained for two steels:

These relationships indicate that the coarse-grained steel is more sensitive to the Z parameter and increases more with increasing temperature and decreasing strain rates. This is due to evolution of finer DRX grains in this steel as a result of the necklace mechanism dominance. As the grains become finer, the cell structure developed interior grains will also be smaller and more homogeneous, which means that the larger volume of the material, participates in the deformation (higher η) [21]. Also, the greater value of m, expresses that the flow localization is more prohibited which, in turn, more ductility is expected.

The power dissipation efficiencies (η) and instability regions are shown in Fig. 4 (e) – (h) for steels with two grain sizes at strains of 0.5 and 0.7. For comparison, Fig. 6 shows the same results obtained for the AISI 304 stainless steel by Venugopal et al. and Tan et al. [13, 22]. It can be seen that there is a good coincidence between the results of the present work and these researchers, both with respect to sth the form and values. A few differences are due to the variations in chemical composition, grain size, and the presence of impurities. It has been reported that, in austenitic stainless steels, impurities even in a small amount, have a considerable effect on the accumulation of dislocations and microstructural changes [23]. Ohadi et al. [24] observed the serrated flow curve in AISI 304L due to segregation of phosphorous.

Some marks have been superimposed on Fig. 5 (e)–(h) to relate the instability regions to the microstructural features. The circle mark indicates that the DRX develops by necklace structure. These regions have been located in the instable zones. This is because, in these conditions, the DRX development is postponed due to the nucleation of the next necklaces of grains from grain boundary of before-necklaces. This consequently, causes minimum power dissipation efficiency. The square sign indicates that cell structure exists, due to dislocation aligning and subgrain formation. Micrographs of Fig. 4 clearly evidence the etch-pits

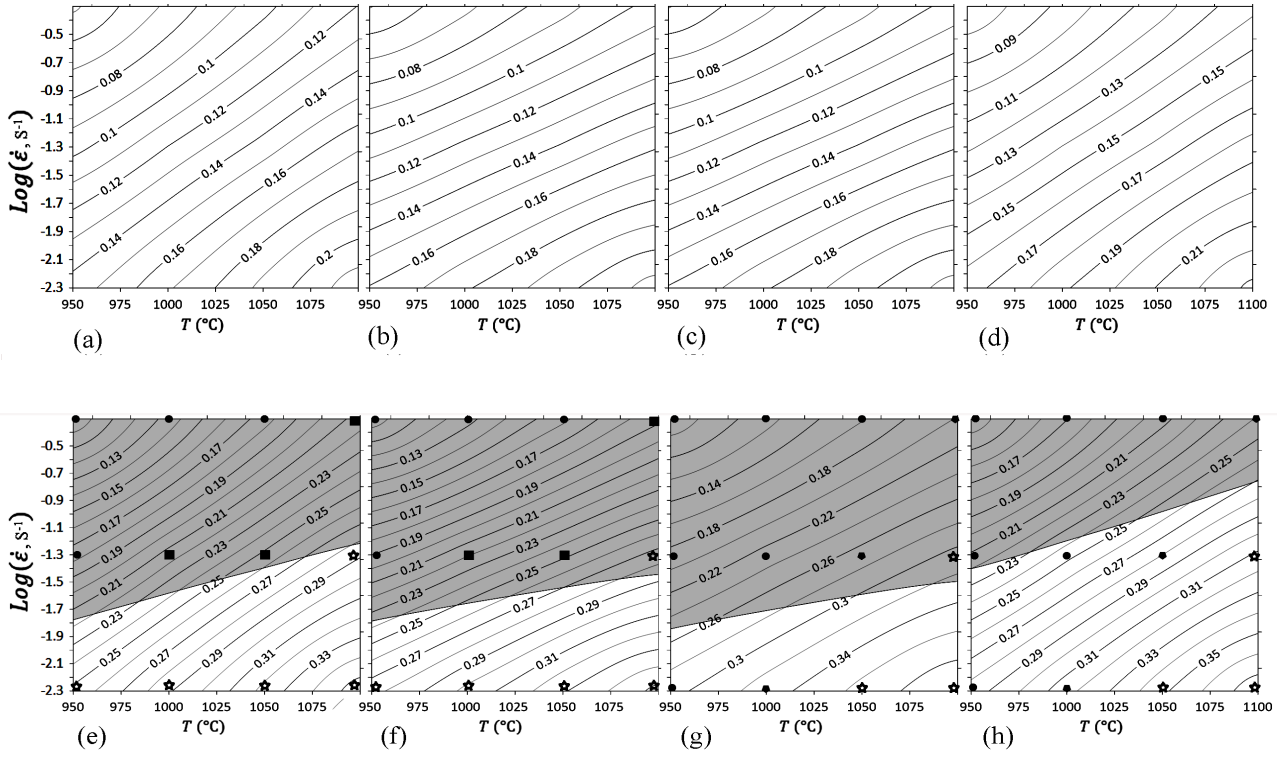

Fig. 5. The strain rate sensitivity (m) in steel with grain size of 15 μm at strains of (a) 0.5 and (b) 0.7, and the same results in steel with grain size of 40 μm at strains of (c) 0.5 and (d) 0.7, and also the power dissipation efficiency (η) in steel with grain size of 15 μm at strains of (e) 0.5 and (f) 0.7, and the same results in steel with grain size of 40 μm at strains of(g) 0.5 and (h) 0.7. The different marks on these figures are indicated as follows: • necklace structure,★no necklace, ■ cell structure interior grains, ● semi-necklace structure.

features. In these conditions, again, power dissipation by microstructure has a medium level. The pentagon mark in diagrams of coarse-grained steel, is relevant to necklace DRX as circle sign, but here due to higher temperature and lower strain rate, the DRX grains strain-hardened more slowly and therefore more time is available for the growth and extension to the grain interiors. In this case, consequently, a heterogeneous structure including fine and coarse grains might be formed. The best results for the maximum power dissipation are related to the DRX evolution with no necklace structure that marks with star sign in these figures. As can be seen, in the steel with finer grain, this region (DRX with no necklace structure) is wider in comparison with the coarser grain sized steel. The same results have been obtained by Ohadi et al. [24] in AISI 304L.

The geometrically necessary dislocations (GNDs) are dislocations with the same burgers vector that facilitate the crystal rotations [25]. These dislocations accumulate near the grain boundary to compensate the non-uniform slip of grains across the grain boundaries due to constraint exertion by neighboring grains. These dislocations can be distributed homogeneously, or locally form dislocation walls. In the latter case, the rotation of the crystals is accumulated in those walls cause an increase in the miss-orientation angle with the increase of the strain [26]. The geometric dislocation density is low as compared to mean dislocation density of grains, but they are not distributed homogenously, therefore the density is only high, along the boundaries in order to compensate the steep gradient of the strain. The density in coarse-grained materials is close to zero, but it is of great importance in fine-grained materials in which by concentrating on the vicinity of the boundaries, creates new grains with high angle boundaries [27]. Fig. 7 shows EBSD (Electron Back-Scattered Diffraction) maps of samples deformed at 900 °C and 0.5 s^{-1} to a strain of 1.0 in steels with grain sizes of 15 and 40 μm. The existence of GNDs near the grain boundary can be clearly seen in the finer grained materials (Fig. 7(b)). These dislocations lead to

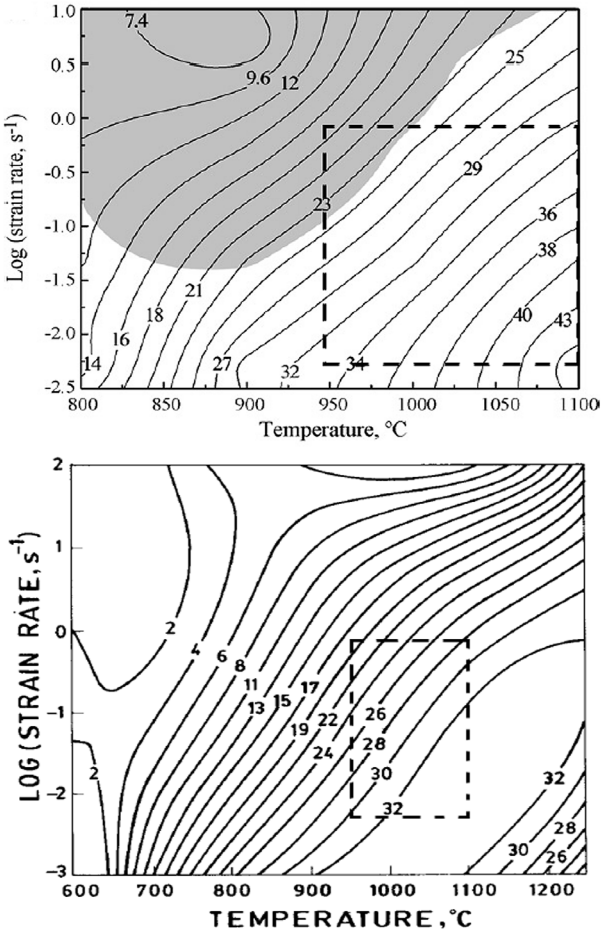

Fig. 6. The power dissipation efficiency and instability maps presented for AISI 304 stainless steel by (a) Tan et al. [22] and (b) Venugopal et al. [13]; the dash lined rectangle shows the window range has been studied in the present work.

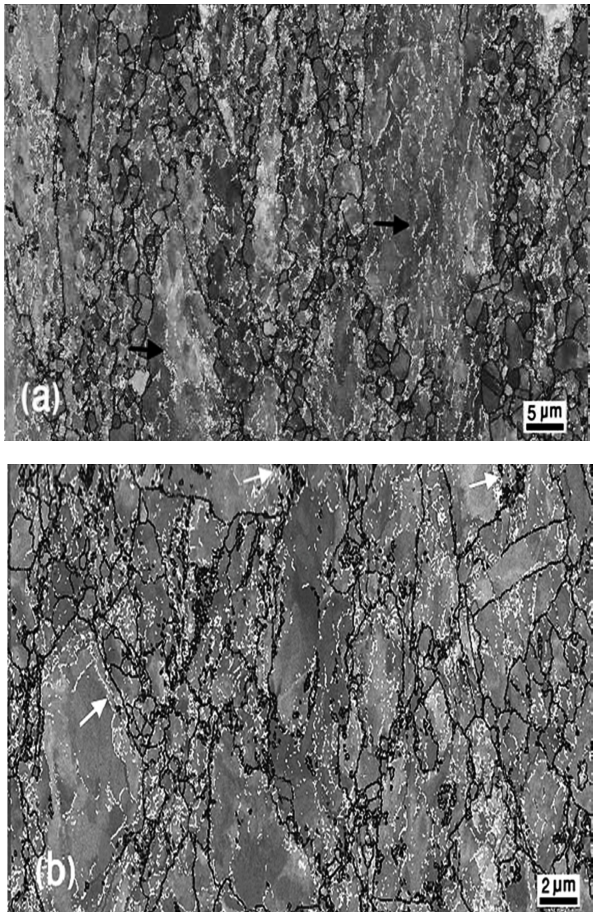

Fig. 7. EBSD maps of samples deformed at 900 ℃ and 0.5 s^{-1} to a strain of 1.0: (a) Coarse-grained material and (b) finer grained material, the existence of GNDs near the grain boundary can be seen in the finer grained material

the development of a more compact cell structure in the vicinity of the boundary and reduce the uniformity of the power dissipation by the microstructure. The presence of this structure is shown in Fig. 5 with a square mark. At the higher temperatures and lower strain rates, the focus on geometric dislocations in fine grain steels decreases and the power dissipation efficiency increases. As the progress of DRX grains, interior the initial grains, was related to evolution of strain induced dislocation sub-boundaries or twinning [28, 29], it seems that the twinning has an important role in the coarser grain steel. As the bulging requires a very high boundary curvature on the existing small recrystallized grains formed in the coarser grain steel, the new DRX grains are formed through the repeated nucleation and growth of annealing twins on the migrating interface. The twin boundaries evolved near the interface of DRX and parent grains might either glide away laterally to the migrating boundary [29]. But in the finer grain steel, the DRX grains are comparatively larger, which bulging can be occurred with the lower boundary curvature and the strain induced dislocation sub-boundaries (or GNDs) can initiate the new DRX grains. More experimental work would be helpful to support this finding.

4. Conclusions

The following results could be withdrawn from the present work:

• Dynamic recrystallization development during hot deformation of AISI 304 stainless steel with two initial grain sizes of 15 and 40 μm has been considered in terms of occurrence of necklace structure. It has been shown that DRX in coarser-grain steel develops further by necklace mechanism and causes the finer grain.

• The strain rate sensitivity obtained in terms of temperature and strain rate and formulated via Z parameter in steels with two initial grain sizes.

• Processing map obtained for steels with two grain sizes. Instability regions have been discussed in coincidence with microstructural evidence. In coarse-grained steel, the existence of necklace structure (or semi-necklace) and in finer-grain steel the development of cell structure interior grains, moreover, the geometrically necessary dislocations near the grain boundaries have been assessed as the metallurgical characteristics caused instability occurrence in the processing maps.

Acknowledgment

The present work has been supported by the vice president of the education and research of the Qom University of Technology (QUT).

References

[1] B. Ahlblom, R. Sandstrom: Int. Met. Rev., 27(1) (1982), 1.
[2] N. D. Ryan, H. J. McQueen: Can. Met. Q., 29(2) (1990), 147.
[3] H. J. McQueen, N. D. Ryan: Stainless Steel ’84, Institute of Metals, London, (1985), 50.
[4] P. V. Sivaprasad, S. Venugopal, Sr. Venugopal, V. Maduraimumuthu, M. Vasudevan, S. L. Mannan, et al.: J. Mater. Process Technol., 132(2003), 262.
[5] S. Venugopal, Sr. Venugopal, P. V. Sivaprasad, M. Vasudevan, S. L. Mannan, S. K. Jha, et al.: J. Mater. Process Technol., 59(1995), 343.
[6] H. Ziegler: Progress in Solid Mechanics, Vol. 4, ed. by I. N. Sneddon and R. Hill, John Wiley and Sons, New York, (1963), 93.
[7] Y. V. R. K. Prasad: Indian J. Technol., 28(1990), 435.
[8] J. Q. Li, J. Liu, Z. S. Cui: Mater. Des., 56(2014), 889.
[9] Y. V. R. K. Prasad, K. P. Rao and S. Sasidhara (eds.): Hot Working Guide—A Compendium of Processing Maps, 2nd ed., ASM International, Materials Park, OH 44073-0002, (2015).
[10] S. R. Keown: Hot working and Forming Processes, ed. by C. M. Sellars and J. D. Davies, Metals Society, London, (1980), 140.
[11] N. D. Ryan, J. McQueen: J. High. Tem. Technol., 8(1) (1990), 27; 8(3) (1990), 185.
[12] J. Rasti, A. Najafizadeh, M. Meratian: Int. J. Mat. Res., 103(2012), 4.
[13] S. Venugopal, S. L. Mannan, Y. V. R. K. Prasad: Mat. Sci. and Eng. A177, (1994), 143.
[14] S. Venugopal, S. L. Mannan, Y. V. R. K. Prasad: Mat. Letters, 15(1992), 79.
[15] K. Huang, R. E. Log: Mater. Des., 9(2016), 12.
[16] K. A. Babu, Y. H. Mozumder, R. Saha, V. S. Sarma, S. Mandal: Mater. Sci. and Eng. A., 7(2018), 104.
[17] R. Ebrahimi, A. Najafizadeh: J. Mater. Proc. Tech., 152(2004), 136.
[18] C. M. Sellars, W. J. McTegart: Acta Metall., 14(1966), 1136.
[19] J. A. Almeida, R. Barbosa: ISIJ Int., 43(2) (2003), 264.
[20] H. Beladi, P. Cizek, P. D. Hodgson: Metall. and Mater. Trans. A., 40A(2009), 1175.
[21] J. R. Foulds, A. M. Ermi, J. Moteff: Mater. Sci. and Eng., 45(1980), 137.
[22] S. Tan, Z. Wang, S. Cheng, Z. Liu, J. Hana, W. Fu: Mater. Sci. and Eng. A., 517(2009), 312.
[23] A. Laasraoui, J. J. Jonas: Metall. Trans. A., 22A(1991), 1545.
[24] D. Ohadi, M. H. Parsa, H. Mirzadeh: Mater. Sci. Eng. A., 565(2013), 90.
[25] A. Belyakov, H. Miura, T. Sakai: Mater. Sci. and Eng. A., 255(1998), 139.
[26] D. Jorge-Badiola, A. Iza-Mendia, I. Guti´errez: Mater. Sci. and Eng. A., A394(2005), 445.
[27] R. Ding, Z. X. Guo: Acta Mater., 49(2001), 3163.
[28] A. Belyakov, H. Miura, T. Sakai: Mate. Sci. Eng. A., 255(1998), 139.
[29] H. Mirzadeh, J. M. Cabrera, A. Najafizadeh, P. R. Calvillo: Mater. Sci. Eng. A., 538(2012), 236.